Inorganic Chemistry

Article

pubs.acs.org/IC

Forward and Reverse (Retro) Iron(III) or Gallium(III) Desferrioxamine E and Ring-Expanded Analogues Prepared Using Metal-Templated Synthesis from *endo*-Hydroxamic Acid Monomers

Tulip Lifa,[†] William Tieu,[†] Rosalie K. Hocking,[‡] and Rachel Codd*[,†]

[†]School of Medical Sciences (Pharmacology) and Bosch Institute, The University of Sydney, Sydney, New South Wales 2006, Australia

[‡]College of Science, Technology & Engineering, James Cook University, Townsville, Queensland 4811, Australia

Supporting Information

ABSTRACT: A metal-templated synthesis (MTS) approach was used to preorganize the forward *endo*-hydroxamic acid monomer 4-[(5-aminopentyl)(hydroxy)amino]-4-oxobutanoic acid (*for*-PBH) about iron(III) in a 1:3 metal/ligand ratio to furnish the iron(III) siderophore *for*-[Fe(DFOE)] (ferrioxamine E) following peptide coupling. Substitution of *for*-PBH with the reverse (retro) hydroxamic acid analogue 3-(6-amino-*N*-hydroxyhexanamido)-propanoic acid (*ret*-PBH) furnished *ret*-[Fe(DFOE)] (*ret*-ferrioxamine E). As isomers, *for*-[Fe(DFOE)] and *ret*-[Fe(DFOE)] gave identical mass spectrometry signals ($[M + H^+]^+$, m/z_{calc} 654.3, m/z_{obs} 654.3), yet *for*-[Fe(DFOE)] eluted in a more polar window (t_R = 23.44 min) than *ret*-[Fe(DFOE)] (t_R = 28.13 min) on a C18 reverse-phase high-performance liquid chromatography (RP-HPLC) column. *for*-[Ga(DFOE)] (t_R = 22.99 min) and *ret*-[Ga(DFOE)] (t_R = 28.11 min) were prepared using gallium(III) as the metal-ion template and showed the same trend for the retention time. Ring-expanded analogues of *for*-[Fe(DFOE)] and *ret*-[Fe(DFOE)] were prepared from *endo*-hydroxamic acid monomers with one additional methylene unit in the amine-containing region, 4-[(6-aminohexyl)(hydroxy)amino]-4-oxobutanoic acid (*for*-HBH) or 3-(7-amino-*N*-hydroxyheptanamido)propanoic acid (*ret*-HBH), to give the corresponding tris(homoferrioxamine E) macrocycles, *for*-[Fe(HHDFOE)] or *ret*-[Fe(HHDFOE)] ($[M + H^+]^+$, m/z_{calc} 696.3, m/z_{obs} 696.4). The MTS reaction using a constitutional isomer of *for*-HBH that transposed the methylene unit to the carboxylic acid containing region, 5-[(5-aminopentyl)(hydroxy)amino]-5-oxopentanoic acid (*for*-PPH), gave the macrocycle *for*-[Fe(HPDFOE)] in a yield significantly less than that for *for*-[Fe(HHDFOE)], with the gallium(III) analogue *for*-[Ga(HPDFOE)] unable to be detected. The work demonstrates the utility and limits of MTS for the assembly of macrocyclic siderophores from *endo*-hydroxamic acid monomers. Indirect measures (RP-HPLC order of elution, *c* log *P* values, molecular mechanics, and density functional theory calculations) of the relative water solubility of the ligands, the iron(III) macrocycles, and the apomacrocycles were consistent in identifying *for*-DFOE as the most water-soluble macrocycle from *for*-DFOE, *ret*-DFOE, *for*-HHDFOE, *ret*-HHDFOE, and *for*-HPDFOE. From this group, only *for*-DFOE is known in nature, which could suggest that water solubility is an important trait in its natural selection.

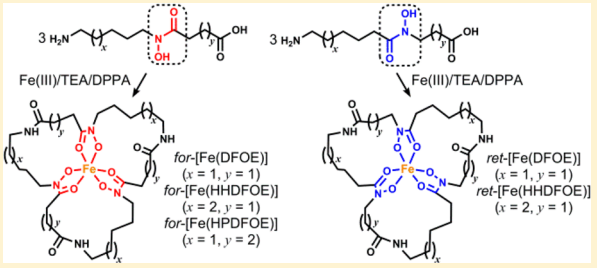

INTRODUCTION

Siderophores are produced by almost all bacteria as agents to increase the bioavailability of iron(III). These organic chelates, which feature different iron(III) binding functional groups [hydroxamic acid, catechol, hydroxycarboxylic acid, and phenolatothia(oxa)zol(id)ines] and different molecular architectures (linear and macrocyclic), leach iron(III) from insoluble oxyhydroxide species or from host transferrin to form more soluble iron(III) siderophore complexes.[1−8] The iron(III) siderophore complex is recognized by receptors at the bacterial cell surface for uptake. The ultimate siderophore-mediated supply of iron to the bacterial cytoplasm enables the assembly of iron-containing proteins essential for survival.[9−13]

The macrocyclic siderophore desferrioxamine E (DFOE) coordinates iron(III) in a 1:1 ratio via three bidentate hydroxamate groups (log K = 32.5) to form ferrioxamine E (FOE).[14−16] DFOE is native to many *Streptomyces* species[9] and other actinomycetes, including marine *Salinispora tropica* CNB-440.[17,18] DFOE is biosynthesized from the condensation and ring closure of three units of the forward *endo*-hydroxamic acid monomer 4-[(5-aminopentyl)(hydroxy)amino]-4-oxobutanoic acid (*for*-PBH).[19−23] Macrocycles are an important class of clinical agents, with research focused on improved chemical or biosynthetic methods to access new candidates.[24−35]

This work has examined the assembly of this trimeric macrocycle in its iron(III)-loaded form, *for*-[Fe(DFOE)], by preorganizing three units of *for*-PBH about iron(III) as a metal-

Received: January 21, 2015
Published: March 19, 2015

ACS Publications © 2015 American Chemical Society

DOI: 10.1021/acs.inorgchem.5b00141
Inorg. Chem. 2015, 54, 3573−3583

ion template, prior to the introduction of peptide coupling reagents (Scheme 1a). The parallel reaction to form reverse

Scheme 1. Forward [*for*-PBH, *for*-HBH, and *for*-PPH (a); *for*-PBH-d_4 (c)] and Retro [*ret*-PBH and *ret*-HBH (b)] *endo*-Hydroxamic Acid Monomers and the Corresponding Iron(III)- or Gallium(III)-Loaded Trimeric Macrocycles

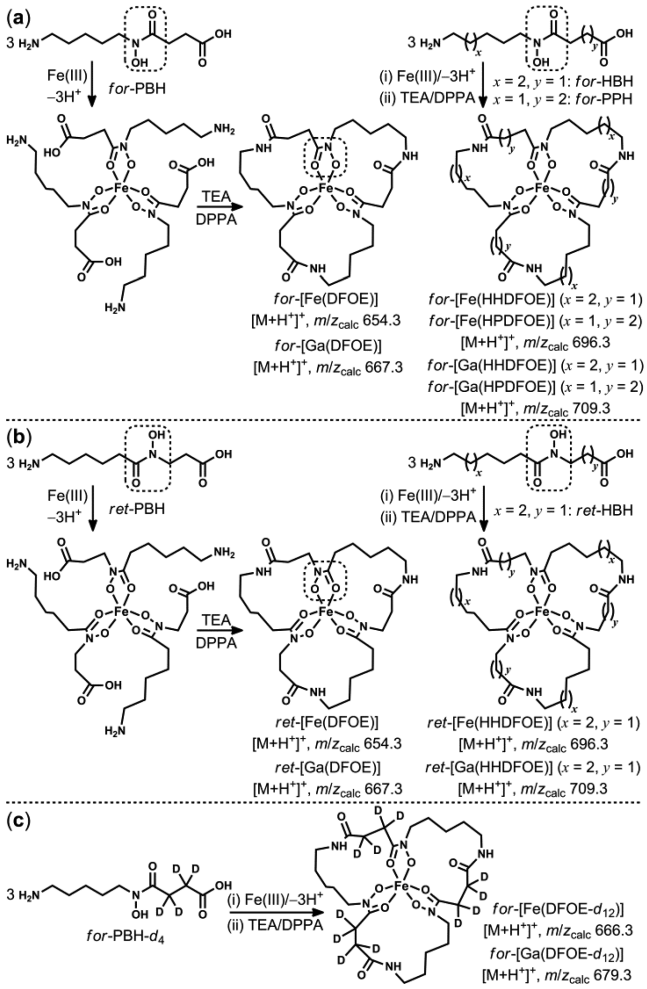

(retro) *ret*-[Fe(DFOE)] was conducted using the retro hydroxamic acid monomer 3-(6-amino-*N*-hydroxyhexanamido)propanoic acid (*ret*-PBH), in which the internal hydroxamic acid motif was reversed relative to the aminocarboxylic acid termini (Scheme 1b). The deuterated 4-[(5-aminopentyl)(hydroxy)amino]-4-oxobutanoic acid-2,2,3,3-d_4 (*for*-PBH-d_4) system was also examined (Scheme 1c).

Our interest in accessing *for*-[Fe(DFOE)] and *ret*-[Fe(DFOE)] was seeded by our preliminary observation of a difference between the energy minima of *for*-[Fe(DFOE)] and *ret*-[Fe(DFOE)], as determined from molecular mechanics (MM) calculations using starting coordinates from X-ray crystallography data (Figure 1).[15,36] This suggested that these isomers might differ in properties that could have functional implications in biology.

Macrocyclic *for*-[Fe(DFOE)] has been synthesized from condensation of the linear precursor *for*-[Fe(DFOG$_1$)], with iron(III) serving to position the terminal amine and carboxylic acid for amide bond formation.[37,38] Previous work prepared *for*-[Fe(DFOE)] and *for*-[Ga(DFOE)] using a metal-templated synthesis (MTS) approach,[39] which inspired the current work

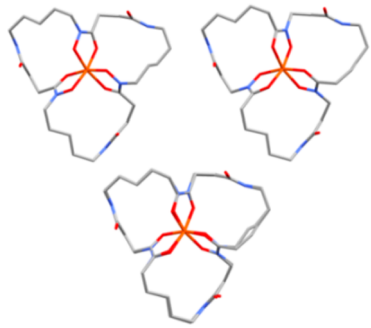

Figure 1. X-ray crystal structures (hydrogen atoms omitted for clarity) of *for*-[Fe(DFOE)][15] (upper left) and *ret*-[Fe(DFOE)][36] (upper right) and the overlay of the two structures (lower). The rms difference for non-hydrogen atoms = 0.1136 Å.

to examine the broader utility of the method. An MTS approach has been used to prepare hydroxamic acid macrocycles with iron(III) used to achieve ring closure via a lactonization reaction.[40] MTS has a rich history in accessing many inorganic and supramolecular complexes.[41−44]

Here, we have established the broader scope of the MTS strategy, as applied to *for*- and *ret*-hydroxamic acid monomers, and for accessing ring-expanded macrocycles using *endo*-hydroxamic acid monomers that contain additional methylene groups in the backbone (Scheme 1). The results demonstrate the utility and limits of MTS for the assembly of macrocyclic siderophores and allow for some insight into factors that might influence the selection of *for*-DFOE in nature.

RESULTS AND DISCUSSION

Synthesis of *endo*-Hydroxamic Acid Ligands. The *endo*-hydroxamic acid aminocarboxylic acid *for*-PBH was prepared, based on literature procedures (Scheme S1 in the Supporting Information, SI),[20,45] with 1,5-dibrompentane used in the first step instead of 1-bromo-5-chloropentane. Substitution of succinic anhydride with succinic anhydride-2,2,3,3-d_4 furnished *for*-PBH-d_4. The succinyl methylene triplet signals at 2.67 and 2.56 ppm in the ^{1}H NMR spectrum of *for*-PBH were absent in that of *for*-PBH-d_4. Substitution of 1,5-dibromopentane with 1,6-dibromohexane furnished 4-[(6-aminohexyl)(hydroxy)-amino]-4-oxobutanoic acid (*for*-HBH). Substitution of succinic anhydride with glutaric anhydride furnished 5-[(5-aminopentyl)(hydroxy)amino]-5-oxopentanoic acid (*for*-PPH).

Reverse or *ret*-hydroxamic acids have been shown to have antimalarial activity[46,47] and are a class of synthetic ligands that attract research interest.[13,48−51] Retro *endo*-hydroxamic acid aminocarboxylic acids were prepared (Scheme 2) using a reaction pathway similar to that described for related compounds.[52] Peptide coupling between 6-Boc-aminohexanoic acid and *tert*-butyl-3-[(benzyloxy)amino]propanoate, the latter as prepared from the Michael addition of *tert*-butyl acrylate and *O*-benzylhydroxylamine, gave an intermediate that after double deprotection furnished *ret*-PBH. Substitution of 6-amino-hexanoic acid with 7-aminoheptanoic acid in the *ret*-PBH synthetic pathway furnished 3-(7-amino-*N*-hydroxyheptanamido)propanoic acid (*ret*-HBH).

All ligands were characterized by electrospray ionization mass spectrometry (ESI-MS), liquid chromatography−mass spectrometry (LC−MS), and ^{1}H and ^{13}C NMR spectroscopy (see the SI). The reverse-phase (RP) LC traces from solutions of the ligands showed single peaks (shoulder on *ret*-HBH), using

DOI: 10.1021/acs.inorgchem.5b00141
Inorg. Chem. 2015, 54, 3573−3583

Scheme 2. Synthesis of *ret*-PBH and *ret*-HBH[a]

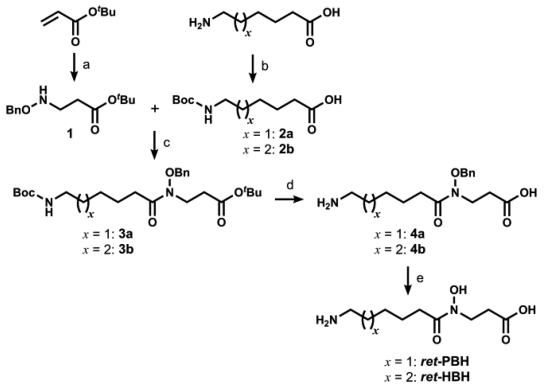

[a](a) BnO-NH_2, TEA, 65 °C; (b) Boc_2O, TEA, THF/H_2O, rt; (c) HOBt, EDC, DMF, rt; (d) 20% TFA/DCM; (e) H_2, Pd/C, ^{t}BuOH/EtOAc, rt.

selected-ion-monitoring (SIM) detection (Figure 2, panels at left). ESI-MS data from bulk solutions (Figure 2, panels at right) showed signals for all of the ligands consistent with the protonated adducts (Table 1).

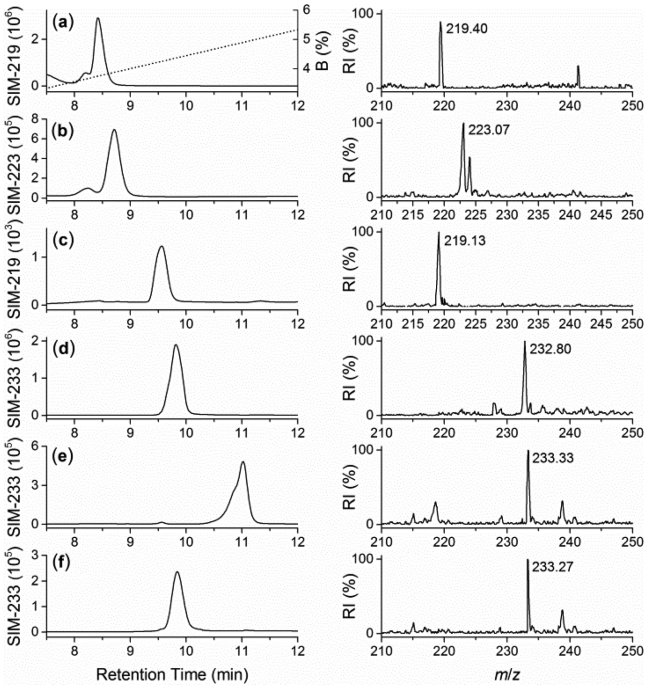

Figure 2. Liquid chromatograms (left column, SIM detection at specified m/z values) and ESI-MS from solutions of (a) *for*-PBH, (b) *for*-PBH-d_4, (c) *ret*-PBH (d) *for*-HBH, (e) *ret*-HBH, or (f) *for*-PPH.

LC−MS Data from Iron(III)-Based MTS Reaction Solutions. The MTS reaction solutions were analyzed by RP LC−MS using the SIM detection mode with the m/z value set to correspond with the target iron(III)-loaded macrocycle (Scheme 1). Isotope patterns were simulated using *ChemCalc*.[53]

A solution of native iron(III)-loaded DFOE, *for*-[Fe(DFOE$_{NAT}$)] (SIM 654), gave a peak in LC at t_R = 24.28 min (Figure 3a). MS analysis of this peak showed three signals (Figure 3a, upper panel in the triad), which simulated (Figure 3a, lower panel in the triad) as the double protonated, protonated, and sodiated adducts of *for*-[Fe(DFOE$_{NAT}$)]

Table 1. LC−MS Data and *c* log *P* Values of the *endo*-Hydroxamic Acid Monomers

				MS signals ([M + H]$^+$)	
ligand	t_R (min)	*c* log *P*	*M* (amu)[a]	m/z_{obs} (RI %)[b]	m/z_{calc}
for-PBH	8.41	−0.40	218.13	219.40 (90.0)	219.13
for-PBH-d_4	8.72	NC[c]	222.15	223.07 (100)	223.16
ret-PBH	9.56	−0.25	218.13	219.13 (100)	219.13
for-HBH	9.82	0	232.14	232.80 (100)	233.15
ret-HBH	11.03	0.14	232.14	233.33 (100)	233.15
for-PPH	9.84	0	232.14	233.27 (100)	233.15

[a]*M*, exact mass. [b]RI, relative intensity (%). [c]NC, not calculated.

(Table 2). The LC−MS trace from the MTS reaction solution between iron(III) and *for*-PBH (SIM = 654) gave a peak at t_R = 23.44 min (Figure 3b), which showed the presence of the same adducts as observed for *for*-[Fe(DFOE$_{NAT}$)], with the double-protonated species appearing as the major adduct. The small difference in the retention time between *for*-[Fe(DFOE$_{NAT}$)] and *for*-[Fe(DFOE)] was due to day-to-day instrumental fluctuations. The integrity of synthetic *for*-[Fe(DFOE)] was verified from LC−MS analysis of a mixed solution of *for*-[Fe(DFOE)] and *for*-[Fe(DFOE$_{NAT}$)], which gave a single peak that analyzed as the target macrocycle.

The MTS reaction solution in which *for*-PBH was replaced with *for*-PBH-d_4 gave a peak at t_R = 23.92 min (SIM 666; Figure 3c). The major signal from MS analysis (100%) was consistent with the double-protonated adduct of *for*-[Fe(DFOE-d_{12})], with a low relative concentration (3%) of the single-protonated adduct (Figure 3c, upper panel in the triad). This supported the veracity of the MTS approach, with preorganization of three *for*-PBH-d_4 monomers about the iron(III) ion template and ring closure, to give the macrocycle ([M + H]$^+$) with an m/z value of 12 units greater than that of *for*-[Fe(DFOE)]. The retention times of *for*-[Fe(DFOE-d_{12})] and *for*-[Fe(DFOE)] were close-to-coincident, as consistent for an ^{2}D−^{1}H analogue pair.

The m/z value of the target macrocycle *ret*-[Fe(DFOE)] (SIM 654) as prepared using MTS from iron(III) and *ret*-PBH, was identical with the value for *for*-[Fe(DFOE)]. The distribution of adducts of *ret*-[Fe(DFOE)] detected by MS (Figure 3d, upper panel in the triad) was similar to that of *for*-[Fe(DFOE$_{NAT}$)] and *for*-[Fe(DFOE)], with one additional double-charged adduct detected ([M + H + K]$^{2+}$, m/z_{calc} 346.6, m/z_{obs} 346.7). There was an increase in the retention time of *ret*-[Fe(DFOE)] (t_R = 28.13 min; Figure 3d) compared to that of *for*-[Fe(DFOE)] (t_R = 23.44 min; Figure 3b).

Analysis of the MTS reaction solution of iron(III) and *for*-HBH, in which one extra methylene group was incorporated in the amine-containing region of the *endo*-hydroxamic acid monomer, gave a peak at t_R = 25.85 min (SIM 696; Figure 3e). This signal was consistent with the presence of *for*-[Fe(HHDFOE)] as a ring-expanded analogue of *for*-[Fe(DFOE)]. The "HH" prefix describes *for*-[Fe(HHDFOE)] as a tris-homo ("H") variant of *for*-[Fe(DFOE)], with the incorporation of additional methylene units in the 1,6-diaminohexane ("H") regions of the molecule. The synthesis of *for*-[Fe(HHDFOE)] shows the broader utility of the MTS approach and the fidelity of the C_3 symmetry of the final macrocycle under these conditions. MS analysis of the peak at t_R = 25.85 min showed signals (Figure 3e, upper panel in the triad) consistent with the presence of the protonated and sodiated adducts of *for*-[Fe(HHDFOE)]. The double-proto-

DOI: 10.1021/acs.inorgchem.5b00141
Inorg. Chem. 2015, 54, 3573−3583

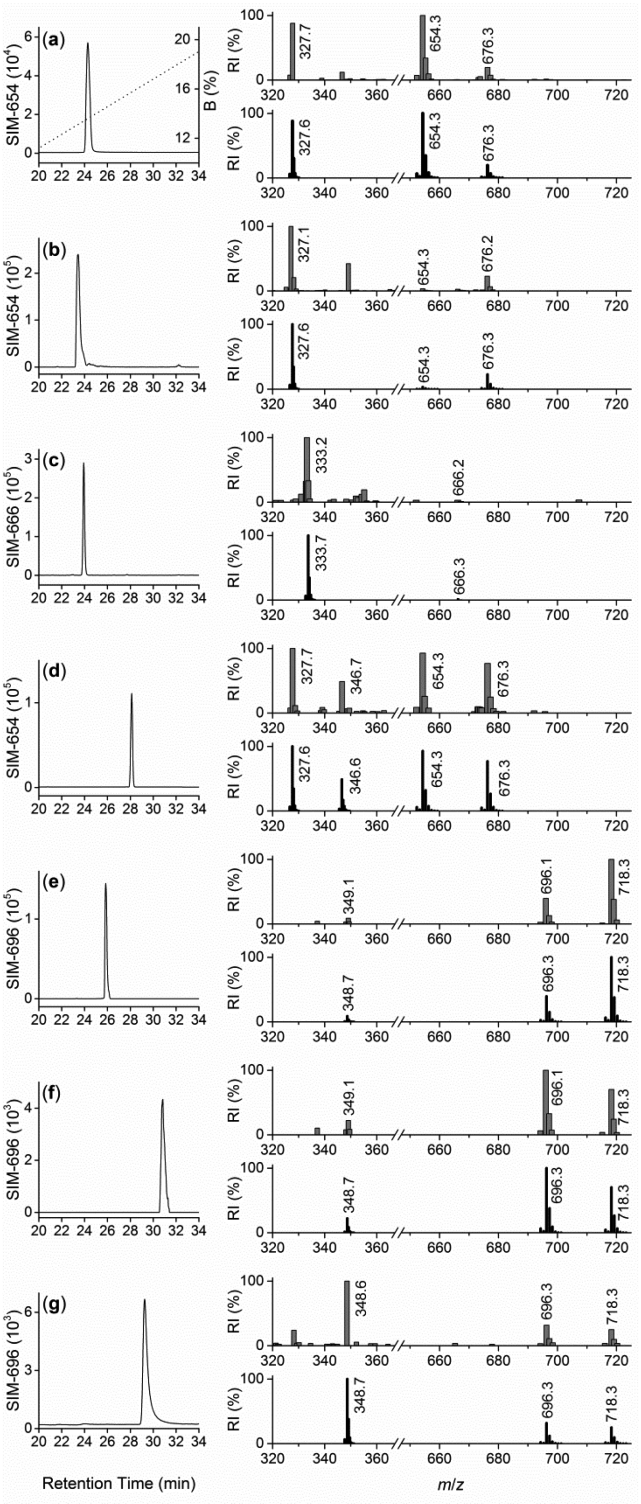

Figure 3. Liquid chromatograms (left column, SIM detection at specified m/z values) and MS spectra from the LC peak maxima [right column, observed (upper panel in the triad, gray); calculated (lower panel in the triad, black)] of (a) authentic *for*-[Fe(DFOE$_{NAT}$)] or from a solution of iron(III) and (b) *for*-PBH, (c) *for*-PBH-d_4, (d) *ret*-PBH, (e) *for*-HBH, (f) *ret*-HBH, or (g) *for*-PPH, after reaction with peptide coupling reagents.

nated adduct was present in low relative concentration (9%). The three additional lipophilic methylene groups present in *for*-[Fe(HHDFOE)] compared to those in *for*-[Fe(DFOE)] were reflected in the values of the retention times of the complexes.

The retention time for the LC peak for *ret*-[Fe(HHDFOE)] (SIM 696; Figure 3f; t_R = 30.84 min) observed from the MTS reaction between iron(III) and *ret*-HBH was greater than that for *for*-[Fe(HHDFOE)]. This trend in the retro isomer eluting later than the forward isomer was the same as that for the *for*-[Fe(DFOE)] and *ret*-[Fe(DFOE)] pair.

In *for*-PPH, an additional methylene group was inserted into the dicarboxylic acid containing region of the ligand. This was achieved in the penultimate reaction step by replacing succinic anhydride with glutaric anhydride. The target MTS macrocycle prepared from iron(III) and *for*-PPH, *for*-[Fe(HPDFOE)] (where "H" refers to tris-homo and "P" refers to 1,5-pentanedioic acid as the region containing the additional methylene group), is a constitutional isomer of *for*-[Fe(HHDFOE)]. The MS signals for *for*-[Fe(HPDFOE)] (Figure 3g, upper panel in the triad) were identical in m/z values with those observed for *for*-[Fe(HHDFOE)] (Figure 3e), with a difference in the relative intensity of the adducts.

Other MTS Reactions. MTS reactions were conducted between iron(III) and equimolar mixtures of *for*-PBH and *for*-PBH-d_4 or *for*-PBH and *ret*-PBH to examine the formation of mixed-ligand iron(III)-loaded macrocycles. No mixed-ligand-type macrocyles were detected by LC–MS or ESI-MS for either of these systems, demonstrating that MTS was competent in furnishing homoleptic but not heteroleptic macrocycles. The essential role of iron(III) in the MTS reaction was confirmed from a metal-free reaction conducted under standard MTS conditions. This reaction solution showed clusters of signals in the ESI-MS trace that could be assigned to linear adducts of *for*-PBH. The intensity of the signals diminished upon the addition of iron(III), which supported the assignment as *for*-PBH and *for*-PBH oligomers. No signals could be assigned to macrocyclic adducts. The critical role of the iron(III) ion for templating the formation of hydroxamic acid macrocycles is supported by previous work that used a macrolactonization ring-closing reaction of a single linear fragment, which was successful only in the presence of iron(III).[40]

LC–MS Data from Gallium(III)-Based MTS Reaction Solutions. The veracity of the MTS approach toward known and new metal-ion-loaded hydroxamic acid macrocycles was supported by equivalent reactions conducted using gallium(III) as the metal-ion template. The presence of the gallium(III)-based analogues *for*-[Ga(DFOE$_{NAT}$)] (Figure 4a), *for*-[Ga(DFOE)] (Figure 4b), *for*-[Ga(DFOE-d_{12})] (Figure 4c), *ret*-[Ga(DFOE)] (Figure 4d), *for*-[Ga(HHDFOE)] (Figure 4e), and *ret*-[Ga(HHDFOE)] (Figure 4f) was evident from the isotope patterns distinct to gallium(III) due to the natural abundance of ^{69}Ga (60.1%) and ^{71}Ga (39.9%).[54,55] In the MTS reaction solution from gallium(III) and *for*-PBH, the peak detected at t_R = 22.99 min (Figure 4b) analyzed in the MS (SIM 667) as four species (Figure 4b, upper panel in the triad) that simulated (Figure 4b, lower panel in the triad) as the double-protonated, protonated potassiated, protonated, and sodiated adducts of *for*-[Ga(DFOE)]. These same adducts were observed for *for*-[Ga(DFOE$_{NAT}$)]. No signal ascribable to *for*-[Ga(HPDFOE)] was detected for the MTS reaction between Ga(III) and *for*-PPH (Figure 4g). The absence of *for*-[Ga(HPDFOE)] and the relatively low levels of *for*-[Fe(HPDFOE)] indicated *for*-PPH was a suboptimal ligand in the MTS system.

DOI: 10.1021/acs.inorgchem.5b00141
Inorg. Chem. 2015, 54, 3573–3583

Table 2. LC−MS Data of *for*-[Fe(DFOE$_{NAT}$)] or *for*-[Ga(DFOE$_{NAT}$)] and from Reaction Solutions between Iron(III) or Galliim(III) and *for*-PBH, *for*-PBH-d_4, *ret*-PBH, *for*-HBH, *ret*-HBH, or *for*-PPH, under Peptide Coupling Conditions

				MS signals for major ions					
				$[M + Na]^+$		$[M + H]^+$		$[M + 2H]^{2+}$	
complex	abbreviation	r_T (min)	M (amu)[a]	m/z_{obs} (RI %)[b]	m/z_{calc}	m/z_{obs} (RI %)	m/z_{calc}	m/z_{obs} (RI %)	m/z_{calc}
[Fe(*for*-DFOE$_{NAT}$)]	*for*-[Fe(DFOE$_{NAT}$)]	24.28	653.3	676.3 (19.4)	676.3	654.3 (100)	654.3	327.7 (87.8)	327.6
[Fe((*for*-PB)$_3$(−H$_2$O)$_3$)]	*for*-[Fe(DFOE)]	23.44	653.3	676.2 (22.7)	676.3	654.3 (3.2)	654.3	327.1 (100)	327.6
[Fe((*for*-PB-d_4)$_3$(−H$_2$O)$_3$)]	*for*-[Fe(DFOE-d_{12})]	23.92	665.3	ND[c]	688.3	666.2 (3.0)	666.3	333.2 (100)	333.7
[Fe((*ret*-PB)$_3$(−H$_2$O)$_3$)]	*ret*-[Fe(DFOE)]	28.13	653.3	676.3 (76.7)	676.3	654.3 (92.7)	654.3	327.7 (100)	327.6
[Fe((*for*-HB)$_3$(−H$_2$O)$_3$)]	*for*-[Fe(HHDFOE)]	25.85	695.3	718.3 (100)	718.3	696.1 (39.5)	696.3	349.1 (8.8)	348.7
[Fe((*ret*-HB)$_3$(−H$_2$O)$_3$)]	*ret*-[Fe(HHDFOE)]	30.84	695.3	718.3 (70.1)	718.3	696.1 (100)	696.3	349.1 (22.2)	348.7
[Fe((*for*-PP)$_3$(−H$_2$O)$_3$)]	*for*-[Fe(HPDFOE)]	29.26	695.3	718.3 (25.0)	718.3	696.3 (31.6)	696.3	348.6 (100)	348.7
[Ga(DFOE$_{NAT}$)]	*for*-[Ga(DFOE$_{NAT}$)]	24.04	666.3	689.3 (17.0)	689.2	667.3 (100)	667.3	334.2 (79.3)	334.1
[Ga((*for*-PB)$_3$(−H$_2$O)$_3$)]	*for*-[Ga(DFOE)]	22.99	666.3	689.2 (33.5)	689.2	667.3 (86.8)	667.3	334.2 (100)	334.1
[Ga((*for*-PB-d_4)$_3$(−H$_2$O)$_3$)]	*for*-[Ga(DFOE-d_{12})]	22.32	678.3	ND[c]	701.3	679.4 (17.3)	679.3	340.2 (100)	340.2
[Ga((*ret*-PB)$_3$(−H$_2$O)$_3$)]	*ret*-[Ga(DFOE)]	28.11	666.3	689.4 (41.1)	689.2	667.3 (100)	667.3	334.2 (97.0)	334.1
[Ga((*for*-HB)$_3$(−H$_2$O)$_3$)]	*for*-[Ga(HHDFOE)]	25.59	708.3	ND[c]	731.3	709.1 (100)	709.3	355.0 (47.2)	355.2
[Ga((*ret*-HB)$_3$(−H$_2$O)$_3$)]	*ret*-[Ga(HHDFOE)]	29.51	708.3	731.3 (100)	731.3	709.4 (58.7)	709.3	355.2 (42.6)	355.2
[Ga((*for*-PP)$_3$(−H$_2$O)$_3$)]	*for*-[Ga(HPDFOE)]	ND[c]	708.3	ND[c]	731.3	ND[c]	709.3	ND[c]	355.2

[a] M = exact mass. [b] RI = relative intensity (%) as normalized to the most intense signal. [c] ND = not detected. Nomenclature: the formation of three peptide bonds between three single-deprotonated *for*-PBH ligands (*for*-PB) is shown within the ultimate bracketed ligand as (−H$_2$O)$_3$. That is, [Fe((*for*-PB)$_3$(−H$_2$O)$_3$)] = *for*-[Fe(DFOE)].

Relative Hydro/Lipophilicity of Ligands and Iron(III) Macrocycles or Apomacrocycles. The order of the retention time of each of the monomers (*for*-PBH < *ret*-PBH < *for*-HBH ~ *for*-PPH < *ret*-HBH) was correlated with its *c* log *P* value (Figure 5). The *c* log *P* value of the apomacrocycle of *for*-[Fe(DFOE)], namely, *for*-DFOE (Table 3), indicated that the macrocycle was more water-soluble than *for*-PBH (Figure 5, downward arrow). The gain in water solubility for the *for*-PBH/*for*-DFOE system was greater than that for the *ret*-PBH/*ret*-DFOE system. In the *ret*-HBH/*ret*-HHDFOE system, the *c* log *P* values indicated that the macrocycle was more hydrophobic than the monomer. There was a minimal difference in the *c* log *P* values of the monomers and macrocycles in the *for*-HBH/*for*-HHDFOE and *for*-PPH/*for*-HPDFOE systems. This indicated that there was a threshold in the size of the macrocycle to maintain water solubility.

The retention time of *ret*-[Fe(DFOB)] indicated that this isomer interacted more strongly with the RP C18 column matrix than *for*-[Fe(DFOB)]. Because these neutral complexes are closely related in structure, the reverse-phase high-performance liquid chromatography (RP-HPLC) retention time can reasonably be used as a surrogate measure of relative lipophilicity.[56] This indicated that *ret*-[Fe(DFOB)] was more lipophilic than *for*-[Fe(DFOB)], which led to the corollary inference that *for*-[Fe(DFOB)] might be more water-soluble than *ret*-[Fe(DFOB)]. This inference was supported by a study showing an inverse relationship (R^2 = 0.72) between the experimentally determined aqueous solubility of a series of related peptides and the RP-HPLC retention factor.[57] The *c* log *P* results suggested that *for*-DFOE was the most water-soluble of the apomacrocycles. From the set of apomacrocycles *for*-DFOE, *ret*-DFOE, *for*-HHDFOE, *ret*-HHDFOE, and *for*-HPDFOE, only *for*-DFOE is known in nature. It is interesting to speculate whether high water solubility might have guided the natural selection of *for*-DFOE.

MM and Density Functional Theory (DFT) Calculations: Ligands. MM calculations were used to provide some insight into the different solvation properties of *for*-PBH and *ret*-PBH, intuited from the RP-HPLC order of elution. These calculations showed a more extensive hydrogen-bonding network existing in the *for*-PBH system solvated with two water molecules (six intermolecular hydrogen bonds; average length 2.209 Å), compared to the *ret*-PBH system (five intermolecular hydrogen bonds; average length 2.233 Å) (Figure 6). Higher-level DFT calculations employing the polarized continuum model (PCM) showed a small but consistent difference in the solvation properties of *for*-PBH and *ret*-PBH. The PCM considers the average solvation effect across a molecule and is a useful comparison to the MM calculations.[58,59] The solvation energy attributed to *for*-PBH or *ret*-PBH was −49.65 or −49.39 kJ mol^{-1}, respectively. The difference in solvation (260 J mol^{-1}) was consistent through three different basis sets (Table S1 in the SI). The Mulliken charges on *for*-PBH and *ret*-PBH show that the differences in charge that lead to differential solvations are small but sufficient to mediate separation (Figure S1 in the SI).

MM Calculations: Complexes. Models of each iron(III)-loaded macrocycle were built using the coordinates from the X-ray crystal structures of *for*-[Fe(DFOE)][15] or *ret*-[Fe(DFOE)].[36] For all complexes, the iron(III) ion and the atoms in the first and second coordination shells were constrained to the coordinates of the corresponding X-ray structure, and the remaining atoms were minimized. The root-mean-square (rms) difference for the 43 non-hydrogen atoms between the X-ray structure of *for*-[Fe(DFOE)] or *ret*-[Fe(DFOE)] and the corresponding minimized structure was 0.1115 or 0.2338 Å, respectively. The average energy minimum of the compounds that contained 36 carbon/nitrogen atoms in the macrocyclic ring system, *for*-[Fe(HHDFOE)], *ret*-[Fe(HHDFOE)], and *for*-[Fe(HPDFOE)], was greater (27.38 kJ mol^{-1}) than that for the macrocycles that contained 33 carbon/nitrogen atoms, *for*-[Fe(DFOE)] and *ret*-[Fe(DFOE)] (23.71 kJ mol^{-1}). The average volume of the ring-expanded macrocycles (1687.4 Å^3) was also greater than that for *for*-[Fe(DFOE)] and *ret*-[Fe(DFOE)] (1553 Å^3).

Of the ring-expanded macrocycles, the model of *for*-[Fe(HPDFOE)] had the smallest volume. This suggested that the low yield of *for*-[Fe(HPDFOE)], compared to that of

DOI: 10.1021/acs.inorgchem.5b00141
Inorg. Chem. 2015, 54, 3573−3583

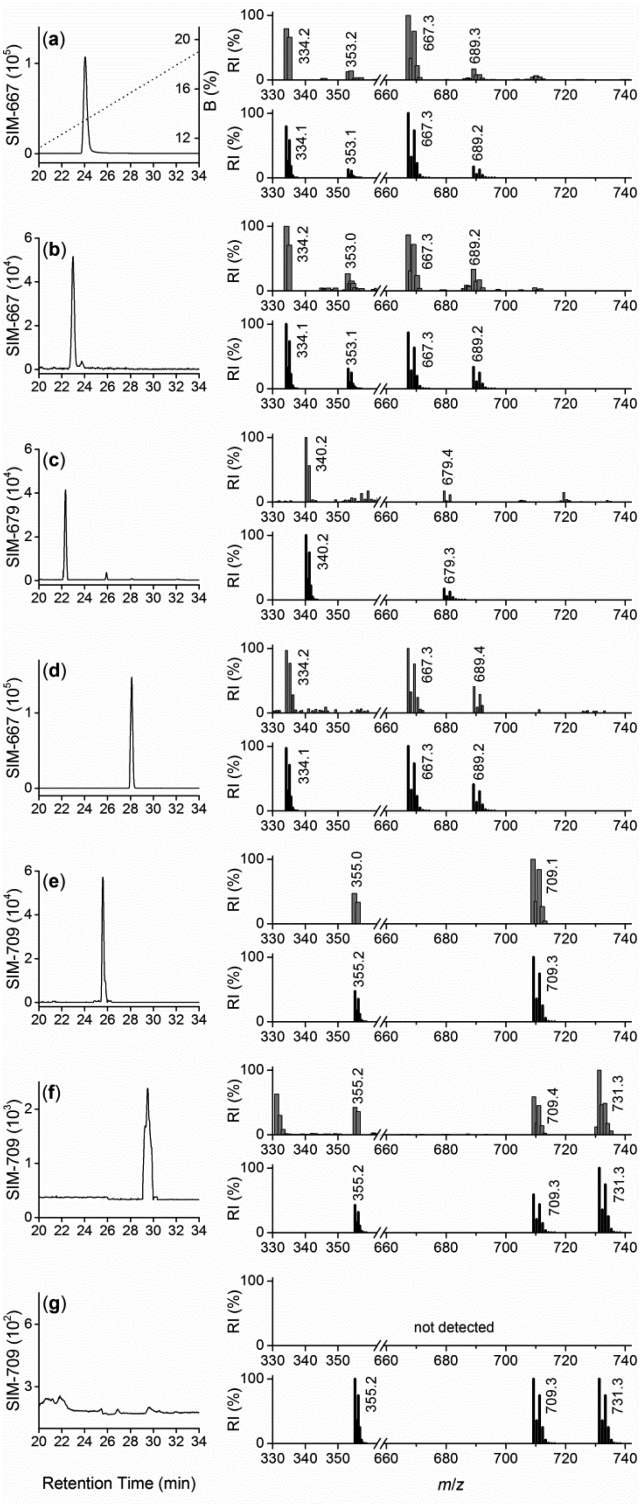

Figure 4. Liquid chromatograms (left column, SIM detection at specified m/z values) and MS spectra from the LC peak maxima [right column, observed (upper panel in the triad, gray); calculated (lower panel in the triad, black)] of (a) authentic *for*-[Ga(DFOE$_{NAT}$)] or from a solution of gallium(III) and (b) *for*-PBH, (c) *for*-PBH-d_4, (d) *ret*-PBH, (e) *for*-HBH, (f) *ret*-HBH, or (g) *for*-PPH, after reaction with peptide coupling reagents.

for-[Fe(HHDFOE)], could be due to intramolecular constraints that reduced the efficiency of ring closure. This notion was examined using models of the precyclized complexes

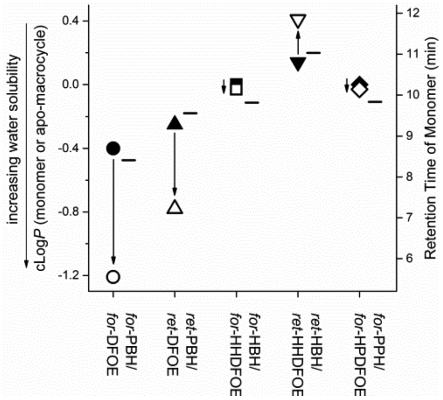

Figure 5. *c* log*P* values (left axis) of *endo*-hydroxamic acid monomers (closed) and the corresponding apomacrocycles (open). The lines represent the retention time of the monomer (right axis).

Table 3. Data from MM Calculations of the Iron(III)-Loaded and -Free (Apo)macrocycles

	energy (kJ/mol)		volume (Å^3)	*c* log *P*
complex	iron(III)	apo	iron(III)	apo
for-[Fe(DFOE)]	26.05	6.15	1548.3	−1.21
ret-[Fe(DFOE)]	21.37	3.89	1557.7	−0.78
for-[Fe(HHDFOE)]	29.70	6.91	1688.1	−0.03
ret-[Fe(HHDFOE)]	24.86	5.03	1695.3	0.41
for-[Fe(HPDFOE)]	27.58	6.22	1678.8	−0.03

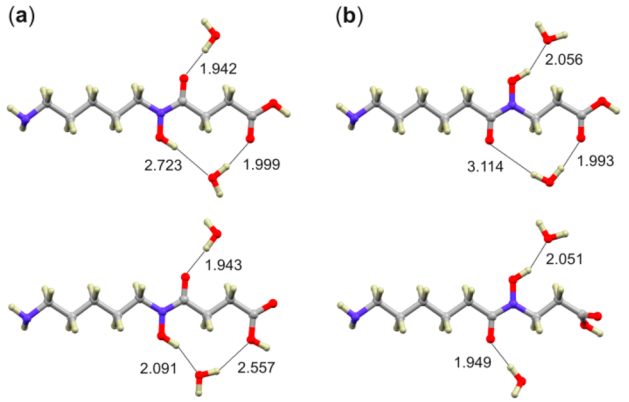

Figure 6. Structures of two solvated *trans* conformers of (a) *for*-PBH or (b) *ret*-PBH, optimized using MM calculations, with hydrogen bond distances (Å) as shown.

between iron(III) and the *endo*-hydroxamic acid monomers with activated acyl azide groups (Figure 7). The minimized model of the precyclized triacyl azide intermediate of [Fe(*for*-PP)$_3$] (Figure 7, left) as the precursor of *for*-[Fe(HPDFOE)] (Figure 7, right) showed that the average distance between the carbonyl carbon atom of ligand 1 and the nitrogen atom of ligand 2 was 3.475 Å. This was the smallest average C(O)···NH$_2$ distance among the precyclized triacyl azide intermediates (Table 4). This was consistent with the inference that this shorter distance could reduce the ring-closure efficiency. It was also possible that part of the constraint arose from the interaction between the carboxylic acid group and iron(III), as posited for a similar system.[40]

The possibility that activation of *for*-PPH was less efficient than that of *for*-HBH or that *for*-PPH had a reduced affinity for iron(III) compared to *for*-HBH was not supported by

DOI: 10.1021/acs.inorgchem.5b00141
Inorg. Chem. 2015, 54, 3573−3583

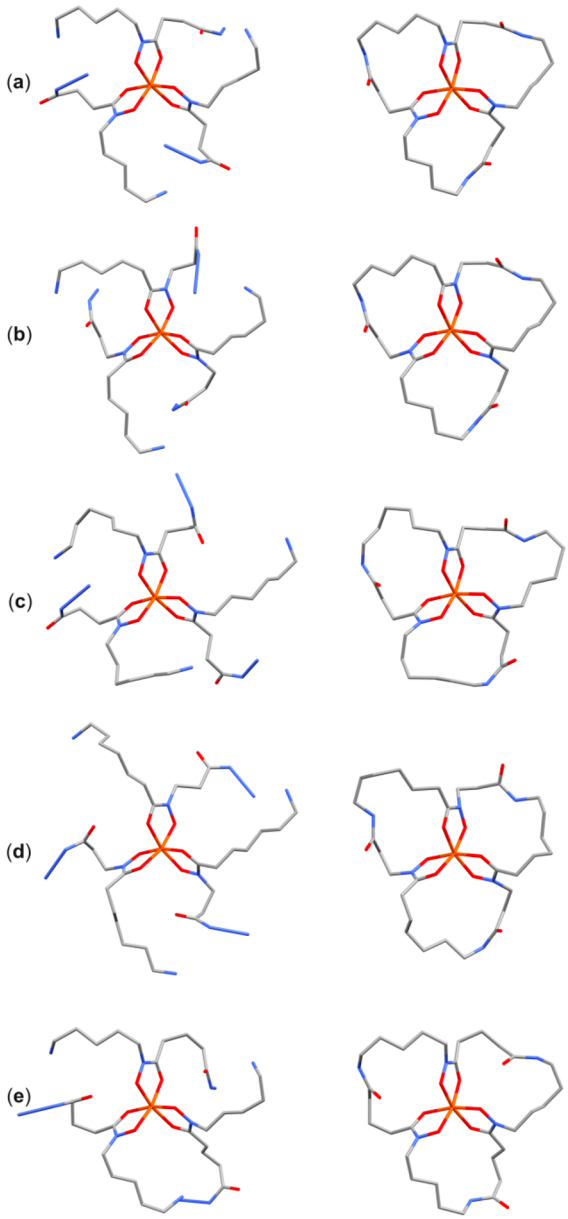

Figure 7. Structures from molecular modeling of precyclized complexes, such as the triacyl azides (left), of (a) Fe(*for*-PB)$_3$, (b) Fe(*ret*-PB)$_3$, (c) Fe(*for*-HB)$_3$, (d) Fe(*ret*-HB)$_3$, and (e) Fe(*for*-PP)$_3$ and the corresponding macrocycles (right).

Table 4. Fragment Distances (Azido Derivatives) from MM Calculations

	distance [$H_2N\cdots C(O)N_3$] (Å)				
complex	1	2	3	av (std)	volume (Å^3)
for-[Fe(DFOE)]	3.626	3.527	3.513	3.555 (0.05)	1548
ret-[Fe(DFOE)]	3.540	3.384	3.991	3.638 (0.26)	1558
for-[Fe(HHDFOE)]	5.664	4.886	3.743	4.764 (0.79)	1688
ret-[Fe(HHDFOE)]	6.775	3.805	6.132	5.571 (1.28)	1695
for-[Fe(HPDFOE)]	3.686	3.350	3.389	3.475 (0.15)	1678

calculations. The activation agents BOP and PyBOP, which have high steric demands, were examined in the ring-closing reaction. Similar to the earlier report,[39] only DPPA was effective, which supported the notion that the preorganized complex had a steric threshold toward viable acyl activation agents.

Siderophore-Mediated Iron Uptake and Siderophore Assembly. In a natural system, a difference in the hydro/lipophilicity between *for*-[Fe(DFOE)] and *ret*-[Fe(DFOB)] could affect the bioavailability. Preferential uptake by the bacterial cell surface receptor of a given iron(III) isomer might be directed by its bioavailability, chirality, and/or constitution (forward/retro). One study showed no detectable difference in the uptake of iron(III)-loaded ferrichrome or *ret*-ferrichrome in *Arthrobacter flavescens*.[49] These results may not be directly applicable to the uptake of *for*-[Fe(DFOE)] and *ret*-[Fe-(DFOE)] by *Streptomyces* sp. because of the positional difference in the hydroxamic acid groups in macrocyclic *exo*-ferrichrome and *endo*-DFOE. Another study showed that the receptor of *Mycelia sterilia* EP-76 recognized only Λ-Cr^{III}-TAFC (TAFC = macrocyclic *endo*-trihydroxamic acid siderophore *N,N′,N″*-triacetylfusarinine C) for uptake, despite the predominance of Δ-Cr^{III}-TAFC in water.[60] The uptake of iron(III) pyochelin by *Pseudomonas aeruginosa* has been shown to be enantioselective, with iron(III) enantiopyochelin not recognized by the FptA receptor.[61] Taken together, these studies demonstrate that the chirality of the iron(III) siderophore complex is a more dominant determinant of uptake than bioavailability. Therefore, it is unlikely that any difference in the bioavailability between *for*-[Fe(DFOE)] and *ret*-[Fe(DFOE)] would have a significant effect on the bacterial iron supply. The effect of constitution in directing uptake has not been established for an endo macrocyclic system, such as *for*-[Fe(DFOE)] and *ret*-[Fe(DFOE)], and is a focus for ongoing work in our group.

The intensity of the signal for *for*-[Fe(HPDFOE)] (SIM = 696, 6.7×10^3 counts; Figure 3g) was significantly less than that for *for*-[Fe(HHDFOE)] (SIM = 696, 1.4×10^5 counts; Figure 3e). Any differences in the purities of the *endo*-hydroxamic acid ligands were not so marked as to explain the 20-fold difference in the intensities in the signals. This indicated that the glutaric acid based *endo*-hydroxamic acid monomer (*for*-PPH) was less effective in the MTS reaction, compared to the succinic acid based monomers (*for*-PBH, *for*-PBH-d_4, and *for*-HBH). In the gallium(III) system, *for*-[Ga(HHDFOE)] was detected, but *for*-[Ga(HPDFOE)] was not. This showed that the position of the additional methylene unit either within the diamine region (*for*-HBH) or within the dicarboxylic acid region (*for*-PPH) influenced the MTS-based assembly. The preference for succinyl- above glutaryl-based macrocycles is reflected in nature, with this class of nonribosomal peptide synthetase-independent siderophore (NIS) assembled from succinyl-coenzyme A (succinyl-CoA)[22,23] and not glutaryl-CoA. The use of glutaryl-CoA in the NIS assembly might have reduced viability because this substrate is used by *Streptomyces* species for the production of extender units for the polyketide synthase (PKS)-dependent biosynthesis of primary and secondary metabolites.[62,63] Succinyl-CoA is also present in higher concentrations than glutaryl-CoA, as part of the tricarboxylic acid or citric acid cycle.[64]

CONCLUSION

The reaction between iron(III) or gallium(III) and a series of *endo*-hydroxamic acid monomers that contained amine and carboxylic acid termini furnished trimeric metal-ion-loaded

DOI: 10.1021/acs.inorgchem.5b00141
Inorg. Chem. 2015, 54, 3573−3583

macrocycles under peptide coupling conditions. With the use of iron(III) as the metal-ion template, the *endo*-hydroxamic acid monomers *for*-PBH, *for*-PBH-d_4, *ret*-PBH, *for*-HBH, *ret*-HBH, and *for*-PPH gave the corresponding macrocycles *for*-[Fe(DFOE)], *for*-[Fe(DFOE-d_{12})], *ret*-[Fe(DFOE)], *for*-[Fe(HHDFOE)], *ret*-[Fe(HHDFOE)], and *for*-[Fe(HPDFOE)]. The use of gallium(III) as the metal-ion template furnished the analogues *for*-[Ga(DFOE)], *for*-[Ga(DFOE-d_{12})], *ret*-[Ga(DFOE)], *for*-[Ga(HHDFOE)], and *ret*-[Ga(HHDFOE)]. The macrocycle *for*-[Ga(HPDFOE)] was not detected. MTS was not an efficient method to prepare significant quantities of hydroxamic acid macrocycles. The merit of the method lies in its ability to provide access to analytical yields of known and new macrocycles and a measure of preference of *endo*-hydroxamic acid monomers suited for the macrocycle assembly.

Indirect measures (RP-HPLC order of elution, *c* log *P* values, and MM and DFT calculations) of the relative water solubility of the ligands, iron(III) macrocycles, and apomacrocycles were consistent in identifying *for*-DFOE as the most water-soluble macrocycle from *for*-DFOE, *ret*-DFOE, *for*-HHDFOE, *ret*-HHDFOE, and *for*-HPDFOE. From this group, only *for*-DFOE is known in nature, which could suggest that water solubility is an important trait in its natural selection.

The relative concentration of *for*-[Fe(HHDFOE)] was greater than that of *for*-[Fe(HPDFOE)]. These ring-expanded analogues of *for*-[Fe(DFOE)] differ only in the position of the additional methylene unit in the diamine or dicarboxylate region, respectively. The greater efficiency of the chemical synthesis of succinyl-based *for*-[Fe(HHDFOE)] above glutaryl-based *for*-[Fe(HPDFOE)] is coincident with the use of succinyl-CoA and not glutaryl-CoA in bacterial NIS biosynthesis.

The macrocycles in this work were trimeric, as directed by the hexadentate coordination preferences of iron(III) and gallium(III). Because zirconium(IV) has a preference for octadentate coordination and forms stable complexes with hydroxamic acid based ligands,[65−68] it is likely that C_4 tetrameric macrocycles would assemble using *endo*-hydroxamic acid monomers in an MTS approach with zirconium(IV) as the metal-ion template. These macrocycles are currently being prepared by our group as ligands for applications in 89-zirconium(IV)-based positron emission tomography imaging.

EXPERIMENTAL SECTION

Reagents: Synthesis of Ligands. The following chemicals were obtained from Sigma-Aldrich: *O*-benzylhydroxylamine hydrochloride (99%), di-*tert*-butyl dicarbonate (Boc_2O; ≥98%), 1,5-dibromopentane (99%), potassium phthalimide (97%), triethylamine (TEA; 99%), 1,4-dioxane (99.8%), tetrahydrofuran (THF; 99.8%), benzylchloroformate (95%), sodium carbonate (99%), sodium hydride (60% suspension in oil), pyridine (99%), sodium sulfite (Na_2SO_3; 99%), succinic anhydride (≥97%), glutaric anhydride (99%), 6-aminohexanoic acid (95%), 7-aminoheptanoic acid (98%), *tert*-butyl acrylate (98%), *N*-[3-(dimethylamino)propyl]-*N*′-ethylcarbodiimide hydrochloride (EDC·HCl; ≥98%), *N*-hydroxysuccinimide (NHS; 98%), *N*,*N*-dimethylformamide (DMF; 99.8%), *tert*-butanol (≥99.0%), and magnesium sulfate ($MgSO_4$; 97%). Trifluoroacetic acid (TFA; ≥98%), silica gel 60 (230−400 mesh), 10% palladium on carbon, and sodium bicarbonate (99.5%) were obtained from Merck. Hydrazine hydrate ($N_2H_4·H_2O$; 99%) was obtained from Ajax Chemicals. *N*,*N*-Ethyldiisopropylamine (DIPEA; 99%) was obtained from Alfa Aesar, *N*-hydroxybenzotriazole (HOBt; ≥99%) was obtained from Auspep, and citric acid (99%) and acetic acid (99.7%) were obtained from Biolab. Hydrogen (H_2) and nitrogen (N_2) gases were sourced from BOC. All chemicals were used as received. Milli-Q water was used for all experiments. DMF was dried over 4 Å molecular sieves. All other solvents, including hexane, ethyl acetate, diethyl ether (99%), dichloromethane (DCM; ≥99.8%), chloroform (99.5%), methanol (99.0%), ethanol (99.5%), and acetonitrile (ACN; 99.9%) as sourced from Ajax Finechem, were used without further purification. Organic extracts were routinely dried with magnesium sulfate. Glassware used for the deprotection of hydroxamates and MTS reactions (below) was soaked in 3 M HCl for 15 min, rinsed with deionized water followed by methanol, and oven-dried prior to use.

Reagents: MTS Reactions. The following additional chemicals were obtained from Sigma-Aldrich: diphenylphosphoryl azide (DPPA; 97%), (benzotriazol-1-yloxy)tripyrrolidinophosphonium hexafluorophosphate (PyBOP; 98%), (benzotriazol-1-yloxy)tris(dimethylamino)-phosphonium hexafluorophosphate (BOP; 97%), $Fe(NO_3)_3·9H_2O$ (99.9%), $Ga(acac)_3$ (99.9%), and $Fe(acac)_3$ (99.9%) [where acac = acetylacetonato]. Authentic samples of *for*-$DFOE_{NAT}$ and *for*-[Fe($DFOE_{NAT}$)] were obtained from EMC Microcollections. A solution of *for*-[Ga($DFOE_{NAT}$)] (0.8 mM) was prepared by dissolving *for*-$DFOE_{NAT}$ (0.5 mg, 0.83 μmol) and $Ga(acac)_3$ (0.3 mg, 0.82 μmol) in 1 mL of methanol.

^{1}H and ^{13}C NMR Spectroscopy. ^{1}H and ^{13}C NMR spectroscopy was carried out using a Varian 400-MR NMR spectrometer (Lexington, MA) at a frequency of 399.73 MHz at 24 °C operated with *VnmrJ 3.1* software (Agilent Technologies, Santa Clara, CA). The spectral data are reported in ppm (δ) from a 2D ACD/NMR processor relative to their residual solvent peaks for $CDCl_3$ (7.27 ppm), D_2O (4.65 ppm), or CD_3OD (3.31 and 4.87 ppm). Coupling constants (J) are reported in hertz. Samples were made to a concentration of 10 mg mL^{-1} in either deuterated chloroform ($CDCl_3$; Cambridge Isotope Laboratory, 99.8%) or deuterated methanol (CD_3OD; Cambridge Isotope Laboratory, 99.8%).

ESI-MS. ESI-MS was conducted using a Finnigan LCQ mass spectrometer (San Jose, CA) with a methanol mobile phase, 0.30 mL min^{-1} flow rate, 25 μL injection volume, 4.50 kV spray voltage, 35 V capillary voltage, 210 °C capillary temperature, and a 10 V tube lens offset.

RP LC−MS. RP-HPLC was conducted using an Agilent Technologies system (Santa Clara, CA), which consisted of a manual injector (20 μL loop), an Eclipse XDB-C18 column (20 μL, 5 μm particle size, 4.6 × 150 mm internal diameter), a binary pump, a diode-array detector, a fraction collector, and a 1260 Infinity degasser. Agilent Chem Station software was used, and conditions were as follows: 0.5 mL min^{-1} flow rate and a 0−28% gradient of ACN in water over 50 min. LC−MS was conducted on the same system with the addition of an autoinjector (10 μL loop) and a 6120 atmospheric pressure chemical ionization mass spectrometer, at a flow rate of 0.4 mL min^{-1}.

RP LC−MS was performed using an Agilent Technologies system (Santa Clara, CA), consisting of an injector (100 μL loop), an Agilent 1260 Infinity degasser, a binary pump, a fraction collector, a diode-array detector, and an Agilent 6120 series quadrupole ESI-MS spectrometer. An Agilent C18 RP prepacked column (5 μm particle size and 4.6 × 150 mm internal diameter) was used with a 0−28% ACN/H_2O gradient over 50 min (A, 99.9:0.1 H_2O/formic acid; B, 99.9:0.1 ACN/formic acid), at a flow rate of 0.5 mL min^{-1}. An Agilent OpenLAB Chromatography Data System ChemStation Edition was used to process mass chromatograms in both the scan and SIM modes.

Synthesis of Ligands. *4-[(5-Aminopentyl)(hydroxy)amino]-4-oxobutanoic Acid (for-PBH).* *for*-PBH was prepared based on literature methods.[20,45] To a solution of 4-[benzyloxy[6-[(benzyloxycarbonyl)amino]hexyl]amino]-4-oxobutanoic acid (60 mg, 0.14 mmol; Schemes S1 and S9 in the SI) in 1:9 (v/v) ethyl acetate/*tert*-butanol (6 mL) was added 10% Pd/C (10 mg). The mixture was stirred under a hydrogen atmosphere (1 atm) for 7 h. The catalyst was filtered and washed with 1:1 (v/v) water/methanol (20 mL), and the filtrate was concentrated in vacuo to give a white solid (28 mg, 95%). ^{1}H NMR (400 MHz, CD_3OD): δ 3.65 (t, J = 6.4 Hz, 2H), 2.90 (t, J = 7.2 Hz, 2H), 2.67 (t, J = 6.8 Hz, 2H), 2.56 (t, J = 6.8 Hz, 2H), 1.61−1.70 (m, 4H), 1.35−1.44 (m, 2H). ^{13}C NMR (101 MHz, CD_3OD): δ 181.0, 175.4, 47.6, 40.5, 34.3, 29.3, 27.9, 26.8, 24.0.

DOI: 10.1021/acs.inorgchem.5b00141
Inorg. Chem. 2015, 54, 3573−3583

ESI-MS (positive-ion mode). Calcd for $C_9H_{18}N_2O_4Na$ ($[M + Na]^+$): m/z 241.09. Found: 241.07 (100%).

4-[(5-Aminopentyl)(hydroxy)amino]-4-oxobutanoic-2,2,3,3-d_4 Acid (for-PBH-d_4). 4-[Benzyloxy[4-(benzyloxycarbonyl)pentyl]-amino]-4-oxo-2,2,3,3-d_4-butanoic acid (61 mg, 0.14 mmol; Schemes S1 and S12 in the SI) was treated with 10% Pd/C (12 mg) following the method described for the preparation of *for*-PBH. The title compound was obtained as a white solid (28 mg, 92%). ^{1}H NMR (400 MHz, CD_3OD): δ 3.65 (t, J = 6.4 Hz, 2H), 2.90 (t, J = 7.2 Hz, 2H), 1.62−1.70 (m, 4H), 1.35−1.43 (m, 2H). ^{13}C NMR (101 MHz, CD_3OD): δ 181.0, 175.4, 47.9, 40.5, 28.0, 26.8, 24.0. ESI-MS (positive-ion mode). Calcd for $C_9H_{15}D_4N_2O_4$ ($[M + H]^+$): m/z 223.09. Found: m/z 223.07 (100%).

4-[(6-Aminohexyl)(hydroxy)amino]-4-oxobutanoic Acid (for-HBH). 4-[Benzyloxy[7-[(benzyloxycarbonyl)amino]heptyl]amino]-4-oxobutanoic acid (41 mg, 0.09 mmol; Schemes S1 and S10 in the SI) was treated with 10% Pd/C (10 mg) following the method described for the preparation of *for*-PBH. The title compound was obtained as a white solid (20 mg, 97%). ^{1}H NMR (400 MHz, CD_3OD): δ 3.63 (t, J = 6.4 Hz, 2H), 2.90 (t, J = 7.6 Hz, 2H), 2.67 (t, J = 7.2 Hz, 2H), 2.52 (t, J = 7.2 Hz, 2H), 1.59−1.70 (m, 4H), 1.30−1.45 (m, 4H). ^{13}C NMR (101 MHz, CD_3OD): δ 180.9, 175.2, 47.7, 40.2, 34.3, 29.5, 28.3, 27.2, 26.3. ESI-MS (positive-ion mode). Calcd for $C_{10}H_{21}N_2O_4$ ($[M + H]^+$): m/z 233.14. Found: m/z 232.80 (100%).

5-[(5-Aminopentyl)(hydroxy)amino]-5-oxopentanoic Acid (for-PPH). 5-[Benzyloxy[5-[(benzyloxycarbonyl)amino]pentyl]amino]-5-oxopentanoic acid (58 mg, 0.13 mmol; Schemes S1 and S11 in the SI) was treated with 10% Pd/C (12 mg) following the method described for the preparation of *for*-PBH. The title compound was obtained as a white solid (29 mg, 98%). ^{1}H NMR (400 MHz, CD_3OD): δ 3.64 (t, J = 6.4 Hz, 2H), 2.91 (t, J = 7.2 Hz, 2H), 2.53 (t, J = 7.2 Hz, 2H), 2.08 (t, J = 7.2 Hz, 2H), 1.85−1.93 (m, 2H), 1.64−1.72 (m, 4H), 1.36−1.44 (m, 2H). ^{13}C NMR (101 MHz, CD_3OD): δ 181.9, 175.8, 48.3, 40.6, 38.2, 32.8, 28.1, 27.1, 24.4, 23.0. ESI-MS (positive-ion mode). Calcd for $C_{10}H_{21}N_2O_4$ ($[M + H]^+$): m/z 233.14. Found: m/z 233.27 (100%).

*tert-Butyl 3-[N-(Benzyloxy)-6-[(tert-butoxycarbonyl)amino]-hexanamido]propanoate (**3a**).* **1** (2.43 g, 9.72 mmol), **2a** (1.87 g, 8.10 mmol), EDC (1.84 g, 9.72 mmol), HOBt (1.30 g, 9.72 mmol), and DIPEA (6.79 mL, 38.88 mmol) were dissolved in DMF (15 mL) and stirred for 24 h. The reaction mixture was diluted with DCM (50 mL) and washed with saturated $NaHCO_3$ (50 mL), water (50 mL), and brine (50 mL). The organic layer was dried over $MgSO_4$, filtered, and concentrated in vacuo. The residue was purified using flash chromatography, eluting with 25% ethyl acetate in hexane to give a clear gum (3.17 g, 84%). ^{1}H NMR (400 MHz, $CDCl_3$): δ 4.70 (s, 2H), 4.62 (bs, 1H), 3.78−3.81 (m, 2H), 2.94−2.99 (m, 2H), 2.40 (t, J = 6.8 Hz, 2H), 2.22 (t, J = 6.8 Hz, 2H), 1.42−1.49 (m, 2H), 1.30−1.37 (m, 11H), 1.30 (s, 9H), 1.13−1.20 (m, 2H). ^{13}C NMR (101 MHz, $CDCl_3$): δ 175.2, 170.9, 156.1, 134.4, 129.4, 129.0, 128.7, 80.9, 79.0, 76.3, 41.5, 40.4, 33.2, 32.3, 29.8, 28.5, 28.0, 26.5, 24.1. ESI-MS (positive-ion mode). Calcd for $C_{25}H_{40}N_2O_6Na$ ($[M + Na]^+$): m/z 487.29. Found: m/z 487.13 (100%).

*tert-Butyl 3-[N-(Benzyloxy)-8-[(tert-butoxycarbonyl)amino]-octanamido]propanoate (**3b**).* **1** (155 mg, 0.62 mmol), **2b** (138 mg, 0.56 mmol), HATU (300 mg, 0.78 mmol), and DIPEA (391 μL, 2.25 mmol) were dissolved in DMF (4 mL) and stirred for 16 h. The reaction mixture was diluted with DCM (50 mL) and washed with saturated $NaHCO_3$ (50 mL), water (50 mL), and brine (50 mL). The organic layer was dried over $MgSO_4$, filtered, and concentrated in vacuo. The residue was purified using flash chromatography, eluting with 25% EtOAc/hexane to give a clear gum (3.17 g, 84%). ^{1}H NMR (400 MHz, $CDCl_3$): δ 7.34−7.38 (m, 5H), 4.80 (s, 2H), 4.54 (bs, 1H), 3.89 (t, J = 6.8 Hz, 2H), 3.04−3.09 (m, 2H), 2.50 (t, J = 7.2 Hz, 2H), 2.31 (t, J = 7.2 Hz, 2H), 1.34−1.60 (m, 22H), 1.90−1.31 (m, 4H). ^{13}C NMR (101 MHz, $CDCl_3$): δ 175.5, 171.0, 156.1, 134.5, 129.4, 129.1, 128.8, 80.9, 79.1, 76.5, 41.7, 40.6, 33.3, 32.5, 30.0, 29.1, 28.6, 28.2, 26.7, 24.5. ESI-MS (positive-ion mode). Calcd for $C_{25}H_{40}N_2O_6Na$ ($[M + Na]^+$): m/z 487.29. Found: m/z 486.93 (100%).

*3-[6-Amino-N-(benzyloxy)hexanamido]propanoic Acid Trifluoroacetic Acid (**4a**).* TFA (1 mL) was added to a solution of **3a** (219 mg, 0.45 mmol) in DCM (4 mL). The solution mixture was stirred for 6 h at room temperature under N_2. The reaction mixture was concentrated in vacuo to give an orange gum (187 mg, 100%). ^{1}H NMR (400 MHz, CD_3OD): δ 7.37−7.43 (m, 5H), 4.87 (s, 2H), 3.96−3.99 (m, 2H), 2.89 (t, J = 7.2 Hz, 2H), 2.57 (t, J = 6.4 Hz, 2H), 2.39 (t, J = 7.2 Hz, 2H), 1.52−1.66 (m, 4H), 1.29−1.37 (m, 2H). ^{13}C NMR (101 MHz, CD_3OD): δ 176.8, 175.0, 135.9, 130.7, 130.0, 129.7, 77.2, 42.3, 40.5, 32.9, 32.6, 28.2, 26.9, 24.9. ESI-MS (positive-ion mode). Calcd for $C_{26}H_{42}N_2O_6Na$ ($[M + Na]^+$): m/z 501.29. Found: m/z 501.21 (100%).

*3-[7-Amino-N-(benzyloxy)heptanamido]propanoic Acid Trifluoroacetic Acid (**4b**).* **3b** (215 mg, 0.42 mmol) was treated with 20% TFA in DCM (5 mL) following the procedure outlined for **4a**. The title compound was obtained as a yellow gum (185 mg, 100%). ^{1}H NMR (400 MHz, CD_3OD): δ 7.37−7.44 (m, 5H), 4.89 (s, 2H), 3.98 (t, J = 6.8 Hz, 2H), 2.89 (t, J = 7.6 Hz, 2H), 2.57 (t, J = 6.8 Hz, 2H), 2.38 (t, J = 6.8 Hz, 2H), 1.49−1.68 (m, 4H), 1.30−1.40 (m, 4H). ^{13}C NMR (101 MHz, CD_3OD): δ 177.1, 175.0, 136.0, 130.8, 130.0, 129.7, 77.2, 42.3, 40.6, 32.7, 29.6, 28.3, 27.1, 25.3, 24.2.

3-(6-Amino-N-hydroxyhexanamido)propanoic Acid (ret-PBH). *ret*-PBH was synthesized, based on the literature for the preparation of similar ligands.[52] To a solution of **4a** (330 mg, 0.99 mmol) in 1:9 (v/v) ethyl acetate/*tert*-butanol (30 mL) was added 10% Pd/C (60 mg). The mixture was stirred under a hydrogen atmosphere (1 atm) for 3 h. The catalyst was filtered and washed with 1:1 (v/v) water/methanol (20 mL), and the filtrate was concentrated in vacuo to give a white solid (230 mg, 94%). ^{1}H NMR (400 MHz, CD_3OD): δ 3.86−3.90 (m, 2H), 2.92 (t, J = 7.6 Hz, 2H), 2.58−2.64 (m, 2H), 2.48−2.52 (m, 2H), 1.61−1.72 (m, 4H), 1.39−1.46 (m, 2H). ^{13}C NMR (101 MHz, CD_3OD): δ 175.8, 175.1, 45.2, 40.5, 32.8, 32.4, 28.3, 27.0, 25.0. ESI-MS (positive-ion mode). Calcd for $C_9H_{19}N_2O_4$ ($[M + H]^+$): m/z 219.13. Found: m/z 219.13 (100%).

3-(7-Amino-N-hydroxyheptanamido)propanoic Acid (ret-HBH). *ret*-HBH was prepared based on the method for *ret*-PBH, with 7-aminoheptanoic acid replacing 6-aminohexamoic acid. To a solution of **4b** (92 mg, 0.27 mmol) in 1:9 (v/v) ethyl acetate/*tert*-butanol (9 mL) was added 10% Pd/C (20 mg). The mixture was stirred under a hydrogen atmosphere (1 atm) for 3 h. The catalyst was filtered and washed with 1:1 (v/v) water/methanol (20 mL), and the filtrate was concentrated in vacuo to give a white solid (81 mg). ^{1}H NMR (400 MHz, CD_3OD): δ 3.71 (t, J = 7.6 Hz, 2H), 2.90−2.94 (m, 2H), 2.60 (t, J = 7.2 Hz, 2H), 2.48 (t, J = 7.6 Hz, 2H), 1.59−1.70 (m, 4H), 1.36−1.46 (m, 4H). ^{13}C NMR (101 MHz, CD_3OD): δ 177.5, 40.7, 34.7, 29.6, 28.3, 27.1, 25.7, 24.2. ESI-MS (positive-ion mode). Calcd for $C_{10}H_{21}N_2O_4$ ($[M + H]^+$): m/z 233.14. Found: m/z 233.33 (100%).

MTS Reactions: General Protocol. The multistep synthesis and purification of the ligands furnished about 10−15 mg of material of sufficient purity to proceed to the MTS reaction. This constrained the scale of the MTS reactions and allowed analytical characterization of reaction solutions. A methanol solution (5 mL) containing 10 mg of a given *endo*-hydroxamic acid monomer (0.046 mmol, *for*-PBH, *for*-PBH-d_4, and *ret*-PBH; 0.043 mmol, *for*-HBH, *ret*-HBH, and *for*-PPH) and $^1/_3$ equiv of M(acac)$_3$ [M = iron(III), *for*-PBH, *for*-PBH-d_4, and *ret*-PBH; M = gallium(III), *for*-PBH, *for*-PBH-d_4, *ret*-PBH, *for*-HBH, *ret*-HBH, and *for*-PPH] or $Fe(NO_3)_3{\cdot}9H_2O$ (*for*-HBH, *ret*-HBH, and *for*-PPH) was stirred at room temperature for 1 h. The solvent was removed, and after drying over P_2O_5, the dark-orange [iron(III)] or pale-yellow [gallium(III)] residue (~14 mg) was dissolved in DMF (10 mL), to which was added a 1:1 mixture of TEA (0.09 mmol) and DPPA (0.09 mmol). After the reaction mixture was stirred at room temperature under N_2 for 7 days, the solvent was removed, and the residue was prepared as a 10 mg mL^{-1} solution in methanol for analysis using ESI-MS, RP-HPLC, and LC−MS.

Calculations: MM. Structures of *for*-PBH and *ret*-PBH with a trans-configured hydroxamic acid group were built in *HyperChem*[69] and minimized using the *AMBER* force field. The positions of two water molecules, placed proximal to the hydrogen-bond donor and acceptor atoms of the hydroxamic acid group [N(OH) and C(O)],

DOI: 10.1021/acs.inorgchem.5b00141
Inorg. Chem. 2015, 54, 3573−3583

were minimized, and the atomic charges were calculated (semi-empirical and CNDO methods). Energy-minimized structures of *for*-[Fe(DFOE)] and *ret*-[Fe(DFOE)] were generated from the respective X-ray crystal coordinates, using the MM+ force field with the following atoms constrained: iron(III) and O_6 (first-coordination shell); C_3 and N_3 (second coordination shell). Structures of *for*-[Fe(HHDFOE)] (additional methylene group inserted between C3 and C4 of the diaminopentane unit) and *for*-[Fe(HPDFOE)] (additional methylene group inserted between C2 and C3 of the 1,4-butanedioic acid unit) were built from *for*-[Fe(DFOE)], and *ret*-[Fe(HHDFOE)] was built from *ret*-[Fe(DFOE)] (additional methylene group inserted between C3 and C4 of the diaminopentane unit), with minimization conditions and constraints as above. The *c* log *P* values for minimized ligands and apomacrocycles were derived from the QSAR function. The acyl azide precyclized complexes were built from the parent minimized structure, with an azide unit installed at the C(O) group, following deletion of the peptide bond. The three $C(O)-N_3$ groups were minimized in isolation in the trans geometry prior to minimization of the complex, using conditions and constraints as above.

Calculations: DFT. The initial optimized structures of *for*-PBH and *ret*-PBH were geometry-optimized using DFT. DFT calculations were performed using *Gaussian09* (revision D.01)[70] with the B3LYP exchange-correlation functional.[71,72] To inform energy differences related to solvation, geometry optimizations were performed in the gas phase and in a PCM.[73−75] Calculations were performed with three different basis sets to demonstrate energy convergence: double-ζ 6-31G*, triple-ζ 6-311G**, and triple-ζ with polarization 6-311++G**. Tight self-consistent-field convergence criteria (10^{-8} au) were used for all calculations. Frequency calculations were performed to ensure that stationary points were minima. The molar entropy, enthalpy, and Gibbs free energy of reactions at 298 K at a pressure of 1 atm were calculated using standard statistical mechanics formulas.[76]

■ ASSOCIATED CONTENT

Supporting Information

Synthetic procedures and ^1H and ^{13}C NMR spectra of *for*-PBH, *for*-PBH-d_4, *ret*-PBH, *for*-HBH, *ret*-HBH, and *for*-PPH, DFT calculations, and Mulliken population analysis. This material is available free of charge via the Internet at http://pubs.acs.org.

■ AUTHOR INFORMATION

Corresponding Author

*E-mail: rachel.codd@sydney.edu.au.

Notes

The authors declare no competing financial interest.

■ ACKNOWLEDGMENTS

The Australian Research Council is acknowledged for research support to R.C. The University of Sydney is acknowledged for the provision of a postgraduate research award (cofunded) to T.L. Dr. Amalie A. H. Pakchung is acknowledged for preliminary contributions to the work. R.K.H. is grateful for an allocation of computing time through the National Computing Merit Allocation Scheme (NCMAS).

■ REFERENCES

(1) Winkelmann, G.; Drechsel, H. In *Products of Secondary Metabolism*; Kleinkauf, H., von Döhren, H., Eds.; VCH: Weinheim, Germany, 1997; Vol. 7, pp 199−246.
(2) Stintzi, A.; Raymond, K. N. In *Molecular and Cellular Iron Transport*; Templeton, D. M., Ed.; Marcel Dekker, Inc.: New York, 2002; pp 273−319.
(3) Sandy, M.; Butler, A. *Chem. Rev.* **2009**, *109*, 4580−4595.
(4) Crumbliss, A. L.; Harrington, J. M. *Adv. Inorg. Chem.* **2009**, *61*, 179−250.
(5) Hider, R. C.; Kong, X. *Nat. Prod. Rep.* **2010**, *27*, 637−657.
(6) Budzikiewicz, H. In *Progress in the Chemistry of Organic Natural Products*; Kinghorn, A. D., Falk, H., Kobayashi, J., Eds.; Springer-Verlag: New York, 2010; Vol. *92*, pp 1−75.
(7) Shanzer, A.; Felder, C. E.; Barda, Y. In *The Chemistry of Hydroxylamines, Oximes and Hydroxamic Acids*; Rappoport, Z., Liebman, J. F., Eds.; John Wiley & Sons, Ltd.: Chichester, England, 2009; pp 751−815.
(8) Zheng, T.; Nolan, E. M. *Metallomics* **2012**, *4*, 866−880.
(9) Müller, G.; Raymond, K. N. *J. Bacteriol.* **1984**, *160*, 304−312.
(10) Neilands, J. B. *J. Biol. Chem.* **1995**, *270*, 26723−26726.
(11) Schalk, I. J.; Hannauer, M.; Braud, A. *Environ. Microbiol.* **2011**, *13*, 2844−2854.
(12) Miethke, M. *Metallomics* **2013**, *5*, 15−28.
(13) Yakirevitch, P.; Rochel, N.; Albrecht-Gary, A. M.; Libman, J.; Shanzer, A. *Inorg. Chem.* **1993**, *32*, 1779−1787.
(14) Anderegg, G.; L'Eplattenier, F.; Schwarzenbach, G. *Helv. Chim. Acta* **1963**, *46*, 1400−1408.
(15) van der Helm, D.; Poling, M. *J. Am. Chem. Soc.* **1976**, *98*, 82−86.
(16) Evers, A.; Hancock, R. D.; Martell, A. E.; Motekaitis, R. J. *Inorg. Chem.* **1989**, *28*, 2189−2195.
(17) Roberts, A. A.; Schultz, A. W.; Kersten, R. D.; Dorrestein, P. C.; Moore, B. S. *FEMS Microbiol. Lett.* **2012**, *335*, 95−103.
(18) Ejje, N.; Soe, C. Z.; Gu, J.; Codd, R. *Metallomics* **2013**, *5*, 1519−1528.
(19) Barry, S. M.; Challis, G. L. *Curr. Opin. Chem. Biol.* **2009**, *13*, 205−215.
(20) Kadi, N.; Oves-Costales, D.; Barona-Gomez, F.; Challis, G. L. *Nat. Chem. Biol.* **2007**, *3*, 652−656.
(21) Kadi, N.; Song, L.; Challis, G. L. *Chem. Commun.* **2008**, 5119−5121.
(22) Challis, G. L. *ChemBioChem* **2005**, *6*, 601−611.
(23) Barona-Gomez, F.; Wong, U.; Giannakopulos, A. E.; Derrick, P. J.; Challis, G. L. *J. Am. Chem. Soc.* **2004**, *126*, 16282−16283.
(24) Driggers, E. M.; Hale, S. P.; Lee, J.; Terrett, N. K. *Nat. Rev. Drug Discovery* **2008**, *7*, 608−624.
(25) White, C. J.; Yudin, A. K. *Nat. Chem.* **2011**, *3*, 509−524.
(26) Marsault, E.; Peterson, M. L. *J. Med. Chem.* **2011**, *54*, 1961−2004.
(27) Wahyudi, H.; Tantisantison, W.; Liu, X.; Ramsey, D. M.; Singh, E. K.; McAlpine, S. R. *J. Org. Chem.* **2012**, *77*, 10596−10616.
(28) Heinis, C. *Nat. Chem. Biol.* **2014**, *10*, 696−698.
(29) Villar, E. A.; Beglov, D.; Chennamadhavuni, S.; Porco, J. A. J.; Kozakov, D.; Vajda, S.; Whitty, A. *Nat. Chem. Biol.* **2014**, *10*, 723−731.
(30) Giordanetto, F.; Kihlberg, J. *J. Med. Chem.* **2014**, *57*, 278−294.
(31) Soe, C. Z.; Codd, R. *ACS Chem. Biol.* **2014**, *9*, 945−956.
(32) Newman, D. J.; Cragg, G. M. In *Macrocycles in Drug Discovery*; Levin, J., Ed.; The Royal Society of Chemistry: Cambridge, U.K., 2015; Vol. *40*, pp 1−36.
(33) Peterson, M. L. In *Macrocycles in Drug Discovery*; Levin, J., Ed.; The Royal Society of Chemistry: Cambridge, U.K., 2015; Vol. *40*, pp 398−486.
(34) Kopp, F.; Marahiel, M. A. *Nat. Prod. Rep.* **2007**, *24*, 735−749.
(35) Kopp, F.; Stratton, C. F.; Akella, L. B.; Tan, D. S. *Nat. Chem. Biol.* **2012**, *8*, 358−365.
(36) Hossain, M. B.; Jalal, M. A. F.; Van Der Helm, D.; Shimizu, K.; Akiyama, M. *J. Chem. Crystallogr.* **1998**, *28*, 53−56.
(37) Keller-Schierlein, W.; Prelog, V. *Helv. Chim. Acta* **1962**, *45*, 590−595.
(38) Bergeron, R. J.; McManis, J. S. *Tetrahedron* **1990**, *46*, 5881−5888.
(39) Kachadourian, R.; Chuilon, S.; Mérienne, C.; Kunesch, G.; Deroussent, A. *Supramol. Chem.* **1997**, *8*, 301−308.
(40) Wencewicz, T. A.; Oliver, A. G.; Miller, M. J. *Org. Lett.* **2012**, *14*, 4390−4393.
(41) Curry, J. D.; Busch, D. H. *J. Am. Chem. Soc.* **1964**, *86*, 592−594.
(42) Fenton, D. E.; Murphy, B. P.; Leong, A. J.; Lindoy, L. F.; Bashall, A.; McPartlin, M. *J. Chem. Soc., Dalton Trans.* **1987**, 2543−2553.

DOI: 10.1021/acs.inorgchem.5b00141
Inorg. Chem. 2015, 54, 3573−3583

(43) Blake, A. J.; Hannam, J. S.; Jolliffe, K. A.; Pattenden, G. *Synlett* **2000**, 1515−1518.
(44) Comba, P.; Curtis, N. F.; Lawrance, G. A.; Sargeson, A. M.; Skelton, B. W.; White, A. H. *Inorg. Chem.* **1986**, *25*, 4260−4267.
(45) Bergeron, R. J.; Liu, Z.-R.; McManis, J. S.; Wiegand, J. *J. Med. Chem.* **1992**, *35*, 4739−4744.
(46) Shanzer, A.; Libman, J.; Lytton, S. D.; Glickstein, H.; Cabantchik, Z. I. *Proc. Natl. Acad. Sci. U.S.A.* **1991**, *88*, 6585−6589.
(47) Golenser, J.; Tsafack, A.; Amichai, Y.; Libman, J.; Shanzer, A.; Cabantchik, Z. I. *Antimicrob. Agents Chemother.* **1995**, *39*, 61−65.
(48) Olsen, R. K.; Ramasamy, K. *J. Org. Chem.* **1985**, *50*, 2264−2271.
(49) Emery, T.; Emery, L.; Olsen, R. K. *Biochem. Biophys. Res. Commun.* **1984**, *119*, 1191−1197.
(50) Kornreich-Leshem, H.; Ziv, C.; Gumienna-Kpntecka, E.; Arad-Yellin, R.; Chen, Y.; Elhabiri, M.; Albrecht-Gary, A.-M.; Hadar, Y.; Shanzer, A. *J. Am. Chem. Soc.* **2005**, *127*, 1137−1145.
(51) Dhungana, S.; Harrington, J. M.; Gebhardt, P.; Möllmann, U.; Crumbliss, A. L. *Inorg. Chem.* **2007**, *46*, 8362−8371.
(52) Suzuki, T.; Ozasa, H.; Itoh, Y.; Zhan, P.; Sawada, H.; Mino, K.; Walport, L.; Ohkubo, R.; Kawamura, A.; Yonezawa, M.; Tsukada, Y.; Tumber, A.; Nakagawa, H.; Hasegawa, M.; Sasaki, R.; Mizukami, T.; Schofield, C. J.; Miyata, N. *J. Med. Chem.* **2013**, *56*, 7222−7231.
(53) Patiny, L.; Borel, A. *J. Chem. Inf. Model.* **2013**, *53*, 1223−1228.
(54) Spasojevic, I.; Boukhalfa, H.; Stevens, R. D.; Crumbliss, A. L. *Inorg. Chem.* **2001**, *40*, 49−58.
(55) Pakchung, A. A. H.; Lifa, T.; Codd, R. *RSC Adv.* **2013**, *3*, 16051−16059.
(56) Henchoz, Y.; Bard, B.; Guillarme, D.; Carrupt, P.-A.; Veuthey, J.-L.; Martel, S. *Anal. Bioanal. Chem.* **2009**, *394*, 707−729.
(57) Gorham, R. D., Jr.; Forest, D. L.; Khoury, G. A.; Smadbeck, J.; Beecher, C. N.; Healy, E. D.; Tamamis, P.; Archontis, G.; Larive, C. K.; Floudas, C. A.; Radeke, M. J.; Johnson, L. V.; Morikis, D. *J. Med. Chem.* **2015**, *58*, 814−826.
(58) Hocking, R. K.; Deeth, R. J.; Hambley, T. W. *Inorg. Chem.* **2007**, *46*, 8238−8244.
(59) Zanith, C. C.; Pliego, J. R., Jr. *J. Comput.-Aided Mol. Des.* **2015**, *29*, 217−224.
(60) Adjimani, J. P.; Emery, T. *J. Bacteriol.* **1988**, *170*, 1377−1379.
(61) Brillet, K.; Reimmann, C.; Mislin, G. L. A.; Noël, S.; Rognan, D.; Schalk, I. J.; Cobessi, D. *J. Am. Chem. Soc.* **2011**, *133*, 16503−16509.
(62) Liu, H.-G.; Reynolds, K. A. *J. Bacteriol.* **1999**, *181*, 6806−6813.
(63) Wilson, M. C.; Moore, B. S. *Nat. Prod. Rep.* **2012**, *29*, 72−86.
(64) Lin, H.; Su, X.; He, B. *ACS Chem. Biol.* **2012**, *7*, 947−960.
(65) Guérard, F.; Lee, Y.-S.; Tripier, R.; Szajek, L. P.; Deschamps, J. R.; Brechbiel, M. W. *Chem. Commun.* **2013**, *49*, 1002−1004.
(66) Deri, M. A.; Ponnala, S.; Zeglis, B. M.; Pohl, G.; Dannenberg, J. J.; Lewis, J. S.; Francesconi, L. C. *J. Med. Chem.* **2014**, *57*, 4849−4860.
(67) Guérard, F.; Lee, Y.-S.; Brechbiel, M. W. *Chem.—Eur. J.* **2014**, *20*, 5584−5591.
(68) Patra, M.; Bauman, A.; Mari, C.; Fischer, C. A.; Blacque, O.; Haussinger, D.; Gasser, G.; Mindt, T. L. *Chem. Commun.* **2014**, *50*, 11523−11525.
(69) *HyperChem-7.5*; Hypercube, Inc.: Gainesville, FL, 2002.
(70) Frisch, M. J.; Trucks, G. W.; Schlegel, H. B.; Scuseria, G. E.; Robb, M. A.; Cheeseman, J. R.; Scalmani, G.; Barone, V.; Mennucci, B.; Petersson, G. A.; Nakatsuji, H.; Caricato, M.; Li, X.; Hratchian, H. P.; Izmaylov, A. F.; Bloino, J.; Zheng, G.; Sonnenberg, J. L.; Hada, M.; Ehara, M.; Toyota, K.; Fukuda, R.; Hasegawa, J.; Ishida, M.; Nakajima, T.; Honda, Y.; Kitao, O.; Nakai, H.; Vreven, T.; Montgomery, J. A., Jr.; Peralta, J. E.; Ogliaro, F.; Bearpark, M. J.; Heyd, J.; Brothers, E. N.; Kudin, K. N.; Staroverov, V. N.; Kobayashi, R.; Normand, J.; Raghavachari, K.; Rendell, A. P.; Burant, J. C.; Iyengar, S. S.; Tomasi, J.; Cossi, M.; Rega, N.; Millam, N. J.; Klene, M.; Knox, J. E.; Cross, J. B.; Bakken, V.; Adamo, C.; Jaramillo, J.; Gomperts, R.; Stratmann, R. E.; Yazyev, O.; Austin, A. J.; Cammi, R.; Pomelli, C.; Ochterski, J. W.; Martin, R. L.; Morokuma, K.; Zakrzewski, V. G.; Voth, G. A.; Salvador, P.; Dannenberg, J. J.; Dapprich, S.; Daniels, A. D.; Farkas, Ö.; Foresman, J. B.; Ortiz, J. V.; Cioslowski, J.; Fox, D. J. *Gaussian09*, revision D.01; Gaussian Inc.: Wallingford, CT, 2009.
(71) Becke, A. D. *J. Chem. Phys.* **1993**, *98*, 5648−5652.
(72) Lee, C.-N.; Yang, W.; Parr, R. G. *Phys. Rev. B* **1988**, *37*, 785−789.
(73) Cammi, R.; Mennucci, B.; Tomasi, J. *J. Phys. Chem. A* **2000**, *104*, 5631−5637.
(74) Cammi, R.; Mennucci, B.; Tomasi, J. *J. Phys. Chem. A* **1999**, *103*, 9100−9108.
(75) Mennucci, B.; Tomasi, J. *J. Chem. Phys.* **1997**, *106*, 5151−5158.
(76) Atkins, P. W. *Physical Chemistry*, 3rd ed.; Oxford University Press: Oxford, U.K., 1986.

DOI: 10.1021/acs.inorgchem.5b00141
Inorg. Chem. 2015, 54, 3573−3583